2-28-2019

A Theoretical Model of Underground Dipole Antennas for Communications in Internet of Underground Things

Abdul Salam
Purdue University, salama@purdue.edu

Mehmet C. Vuran

Xin Dong

Christos Argyropoulos

Suat Irmak

A Theoretical Model of Underground Dipole Antennas for Communications in Internet of Underground Things

Abdul Salam, *Member, IEEE,* Mehmet C. Vuran, *Member, IEEE*, Xin Dong, Christos Argyropoulos, *Senior Member, IEEE* and Suat Irmak

***Abstract*—The realization of Internet of Underground Things (IOUT) relies on the establishment of reliable communication links, where the antenna becomes a major design component due to the significant impacts of soil. In this paper, a theoretical model is developed to capture the impacts of change of soil moisture on the return loss, resonant frequency, and bandwidth of a buried dipole antenna. Experiments are conducted in silty clay loam, sandy, and silt loam soil, to characterize the effects of soil, in an indoor testbed and field testbeds. It is shown that at subsurface burial depths (0.1-0.4m), change in soil moisture impacts communication by resulting in a shift in the resonant frequency of the antenna. Simulations are done to validate the theoretical and measured results. This model allows system engineers to predict the underground antenna resonance, and also helps to design an efficient communication system in IOUT. Accordingly, a wideband planar antenna is designed for an agricultural IOUT application. Empirical evaluations show that an antenna designed considering both the dispersion of soil *and* the reflection from the soil-air interface can improve communication distances by up to five times compared to antennas that are designed based on *only* the wavelength change in soil.**

***Index Terms*—Underground Antenna, Cyber-physical systems, Underground electromagnetic propagation, Wireless underground sensor networks, Precision agriculture.**

I. Introduction

INTERNET of underground things (IOUT) are a natural extension of Internet of Things (IoT) to underground settings. IOUTs include sensor motes that are buried in soil and provide applications in precision agriculture [18], [48], [50], [51], [53], [54], [65], border patrol, pipeline monitoring, environment monitoring [1], [46], [52], [68], [69], [73], [75], [83], and virtual fencing [4]. The main challenge towards the realization of IOUT is the establishment of reliable wireless communication links. In this aspect, several challenges exist for the design of an antenna that is suitable for underground (UG) communication. Particularly, input impedance of the UG antenna is a function of soil properties, soil moisture, operation frequency, and burial depth [86].

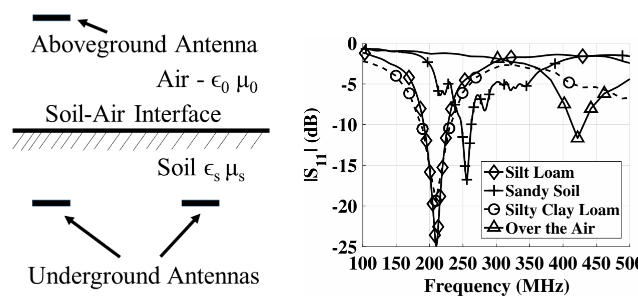

(a) Buried antennas (b) Return loss of a UG antenna

Fig. 1: Underground Communications Scenario.

In this paper, we consider three major factors that impact the performance of a buried antenna. First, due to higher permittivity and frequency dispersion of soil compared to that of air, the wavelength of the electromagnetic wave propagating in soil is significantly different than that in air. Second, soil moisture changes over time with the natural precipitation or irrigation, which dynamically impacts the permittivity of soil. This causes variations in the antenna wavelength. Third, a unique challenge is posed by the difference in electromagnetic wave propagation mechanism in underground and aboveground communications links (Figs. 1). In underground to underground link, lateral wave [38] is the most dominant contributor of the received signal strength at the receiver [11], [48], [49]. Lateral wave travels along the surface and continuously makes ingress to the soil to reach the receiver. It suffers lowest attenuation as compared to other direct and reflected components which have their total path through the soil. Due to these factors, an impedance matched antenna for over-the-air (OTA) communication will not be matched in soil (Fig 1(b)) and separate antenna designs are required for optimal underground and aboveground communication links. Our experiments show that these changes in wavelength is an important factor to consider in the design of an underground antenna. In Fig. 1(b), when a 433 MHz dipole antenna is buried underground, a 47 % (229 MHz) shift in resonant frequency can be observed in silt loam soil in comparison to OTA case. Therefore, an underground communication system should be designed to account for this shift due to soil medium. Moreover, the variations in wavelength over different soil moisture values dictate that an underground antenna should accommodate a

A. Salam is with the Department of Computer and Information Technology, Purdue University, West Lafayette, IN 47907 (e-mail: salama@purdue.edu).

M. C. Vuran is with the Department of Computer Science and Engineering, University of Nebraska-Lincoln, Lincoln, NE (e-mail: mcvuran@cse.unl.edu).

Xin Dong is a member of technical staff at Riverbed Technology.

Christos Argyropoulos is with Department of Electrical Engineering, University of Nebraska-Lincoln, Lincoln, NE 68588 Email: christos.argyropoulos@unl.edu.

Suat Irmak is with Department of Biological Systems Engineering, University of Nebraska-Lincoln, Lincoln, NE 68583 Email: sirmak2@unl.edu.

This work is supported in part by NSF grants NSF CNS-1619285, DBI-1331895, and NSF CNS-1423379.

Manuscript received April 10, 2018; revised December 4, 2018, accepted February 17, 2019.

wide range of wavelengths.

In this paper, we first develop an UG antenna impedance model to capture these effects on buried dipole antennas. The model is then compared with simulations and experimental results. Experiments are conducted using antennas buried in silt loam, sandy, and silty clay loam to verify the impact of soil moisture and burial depth on the performance of dipole antenna in three different types of soil. Based on the insight gathered from the experiments, it is highlighted that for the design of an underground antenna, it is desirable to have the ability to adjust its operation parameters such as radiation pattern, and operation frequency based on dynamic changes in soil moisture.

To the best of our knowledge, no return loss measurements are available to show the impact of soil-air interface, soil properties, and soil moisture on the return loss of underground dipole antenna and this is the first work to present this analysis. The rest of the paper is organized as follows: In Section II, related work on communication in medium and the impact of the medium on antenna impedance is introduced. The impedance and the return loss of dipole antenna buried in soil are analyzed theoretically in Section III, where an antenna impedance model is developed. Underground antenna simulations and experiments setup is presented in Section IV. Validation of theoretical, simulated and measured results are shown in Section V. The paper is concluded in Section VII.

II. Related Work

Antennas used in IOUT are buried in soil, which is uncommon in traditional communication scenarios. Over the entire span of 20^{th} century, starting from Sommerfeld's seminal work [61] in 1909, electromagnetic wave propagation in subsurface stratified medias has been studied extensively [6], [7], [9], [17], [30], [42], [66], [70], [82], [84], and effects of the medium on electromagnetic waves has been analyzed. However these studies analyze fields of horizontal infinitesimal dipole of unit electric moment, whereas for practical applications, a finite size antenna with known impedance, field patterns, and current distribution is desirable. Here, we briefly discuss major contributions of this literature. Field calculations and numerical evaluation of the dipole $over$ the lossy half space are first presented in [43]. EM Wave propagation $along$ the interface has been extensively analyzed in [82]. However, these studies can not be applied to antennas buried underground. Analysis of a the dipole buried in a lossy half space is presented in [42]. By using two vector potentials, the depth attenuation factor and ground wave attenuation factor of far-field radiation form UG dipole was given. However, reflected current from soil-air interface is not considered in this work. In [7], field components per unit dipole moment are calculated by using the Hertz potential which were used to obtain the EM fields. The work in [42] differs from [7] on the displacement current in lossy half space, where former work does not consider the displacement current. In [70], fields from a Hertzian dipole immersed in an infinite isotropic lossy medium has been given. King further improved EM fields by taking into account the half-space interface and lateral waves [38], [85]. In King's work, complete EM fields, from a horizontal infinitesimal dipole with unit electric moment immersed in lossy half space, are given at all points in both half spaces at different depths. Since buried UG antennas are extended devices, fields generated from these antennas are significantly different from the infinitesimal antennas.

Antennas in matter have been analyzed in [23], [24], [37], where the EM fields of antennas in infinite dissipative medium and half space have been derived theoretically. In these analyses, dipole antennas are assumed to be perfectly matched and hence the return loss is not considered. In [30], [84] radiation efficiency and relative gain expressions of underground antennas are developed but simulated and empirical results are not presented. In [32], the impedance of a dipole antenna in solutions are measured. The impacts of the depth of the antenna with respect to the solution surface, the length of the dipole, and the complex permittivity of the solution are discussed. However, this work cannot be directly applied to IOUTs since the permittivity of soil has different characteristics than solutions and the change in the permittivity caused by the variations in soil moisture is not considered. Communications between buried antennas have been discussed in [35], but effects of antennae orientation and impedance analysis has not been analyzed. Performance of four buried antennas has been analyzed [22], where antenna performance in refractory concrete with transmitter buried only at single fixed depth of 1 m without consideration of effects of concrete-air interface is analyzed. In [12], analysis of circularly polarized patch antenna embedded in concrete at $3\,\mathrm{cm}$ depth is done without consideration of the interface effects.

In existing IOUT experiments and applications, the permittivity of the soil is generally calculated according to a soil dielectric model [3], [44], which leads to the actual wavelength at a given frequency. The antenna is then designed corresponding to the calculated wavelength [75]. In [75], an elliptical planar antenna is designed for an IOUT application. The size of the antenna is determined by comparing the wavelength in soil and the wavelength in air for the same frequency. However, this technique does not provide the desired impedance match. In [86], experimental results are shown for Impulse Radio Ultra-Wide Band (IR-UWB) IOUT, however impact of soil-air interface is not considered. In [77], a design of lateral wave antenna is presented where antennas are placed on surface but underground communication scenario is not considered. Closed form expressions to predict the resonance frequency of the microstrip, and patch antennas have been proposed in [5], [87], that only take into account the antenna substrate properties and dimensions, but dispersion of the surrounding medium and boundary effects are not considered.

Another approach being used for wireless underground communications is Magnetic Induction (MI) [1], [2], [26], [27], [40], [67], [71], [81], which is based on the use of coils as radiating devices and these have different propagation characteristics as compared to the underground IOUT antenna. Magnetic induction techniques have several limitations. Signal strength decays with inverse cube factor and high data rates are not possible. Moreover, in MI, communication cannot take place if sender receiver coils are perpendicular to each other. Network architecture cannot scale due to very long wavelengths of the magnetic channel. Therefore, due to these limitations and its inability to communicate with above-ground devices, this approach cannot be readily implemented in IOUT.

In [28], the current distribution and impedance properties of dipole elements in a large subsurface antenna array are derived and compared with experimental data. However, this analysis assumes a homogeneous conducting medium with a large loss tangent with array immersed in a tank containing salt solution, which is not the case in soil. The disturbance caused by impedance change in soil is similar to the impedance change of a hand-held device close to a human body [8], [76] or implanted devices in human body [15], [25]. In these applications, simulation and testbed results show that there are impacts from human body that cause performance degradation of the antennas. Though similar, these studies cannot be applied to the underground communication directly. First, the permittivity of the human body is higher than in soil. At $900\,\mathrm{MHz}$, the relative permittivity of the human body is 50 [76] and for soil with a soil moisture of 5%, it is 5 [44]. In addition, the permittivity of soil varies with moisture, but for human body, it is relatively static. Most importantly, in these applications, the human body can be modeled as a block while in underground communications, soil is modeled as a half-space since the size of the field is significantly larger than the antenna.

To the best of the our knowledge, no existing work takes into account the soil type and soil moisture variations on the underground antenna characteristics, and soil-air interface effects on antenna input impedance. Major contribution of this work is the development and validation of a resonant frequency model to predict resonance under different soil moisture levels in different soil types at different depths. This knowledge of shift of resonant frequency of UG antenna for different soil moisture levels is also useful to determine the transmission loss due to antenna mismatch in IOUT communications

Since, main emphasis of this paper is on the finding resonance for different soil types, depths, soil moisture levels and choosing the right wavelength for IOUT communications, therefore, impedance matching problem is not considered in this work. As depth and soil moisture variations affect the wide range of frequencies, it is challenging to achieve broadband matching over this wide spectrum and leads to performance degradation [15]. Moreover, the model and analysis in this work applies only to antennas buried up to $1\,\mathrm{m}$ depth, because of the considered application, such as in precision agriculture devices are buried in this depth range. In this depth, due to close proximity to surface, soil-air interface plays an important role.

III. System Model

In this section, first, input impedance of a UG antenna is modeled as a function of soil properties and soil moisture by defining the wavenumber in soil, and then, other important parameters of the UG antenna such as resonant frequency, and bandwidth are derived.

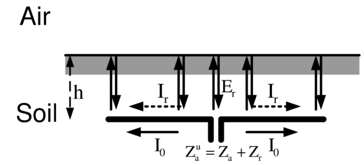

(a) Buried antenna in the half-space

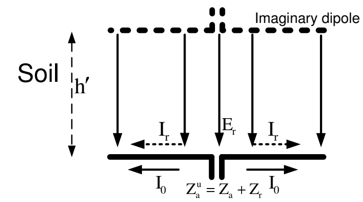

(b) The mutual impedance model

Fig. 2: The analysis of the impedance of a buried dipole antenna.

A. Terminal Impedance of Underground Dipole Antenna as a Function of Soil Properties

Antenna impedance, Z_a, is the ratio of voltage and current at the same point on driving point of the antenna. Complex power radiated by antenna can be calculated by integrating Poynting's vector $\mathbf{S} = \mathbf{E} \mathbf{X} \mathbf{H}$, that gives the energy flow intensity at some point in field, over the enclosing surface of antenna. It is given as [23]:

$$Z_a = \frac{1}{I^2} \int \int \mathbf{E} \ \mathbf{X} \ \mathbf{H} \ . \ \mathbf{da} \ , \tag{1}$$

where I is antenna current, $\mathbf{da}$ is perpendicular in the direction of surface of antenna. For a perfectly conducting antenna, it can be assumed that other than antenna feeding region $\mathbf{E}(\mathbf{x}, \mathbf{y}, \mathbf{z}) \equiv \mathbf{0}$. Then impedance is ascertained by integration of surface current density and tangential electric field over antenna enclosing surface. Then, (1) becomes [23]:

$$Z_a = \frac{1}{I^2} \int \int \mathbf{E} \ \mathbf{X} \ \mathbf{J_{se}} \ . \ \mathbf{da} \ , \tag{2}$$

where $\mathbf{J_{se}}$ is surface current density. By using the induced EMF method [21], (2) can be rewritten as:

$$Z_a = -\frac{1}{I(0)^2} \int_{-l}^{l} \mathbf{E_z} \ \mathbf{I}(\zeta) \ \mathbf{d}\zeta \ , \tag{3}$$

By using (3), the self-impedance of the underground dipole antenna is determined by calculating the electric field $\mathbf{E_z}$ produced by an assumed current distribution $\mathbf{I(0)}$. Accordingly, current and electric field is integrated over the antenna surface.

To model the impedance and return loss of a buried antenna, we consider the antenna in a homogeneous soil. In this setting, the impacts of the soil properties on the impedance are captured. First, however, it is important to consider the wavenumber. The dispersion[1] in soil is given in Appendix A.

Current distribution on antenna is a function of radiation and absorption in soil, which in turn depends on the dielectric properties of the soil. In stratified media, it is difficult to measure current distribution with high accuracy [23]. In [37],

[1] Another approximation of the complex wavenumber is given in [36], which involves Fourier transform of the Bessel function kernel $K(z)$. A similar wavenumber has also been presented in [82].

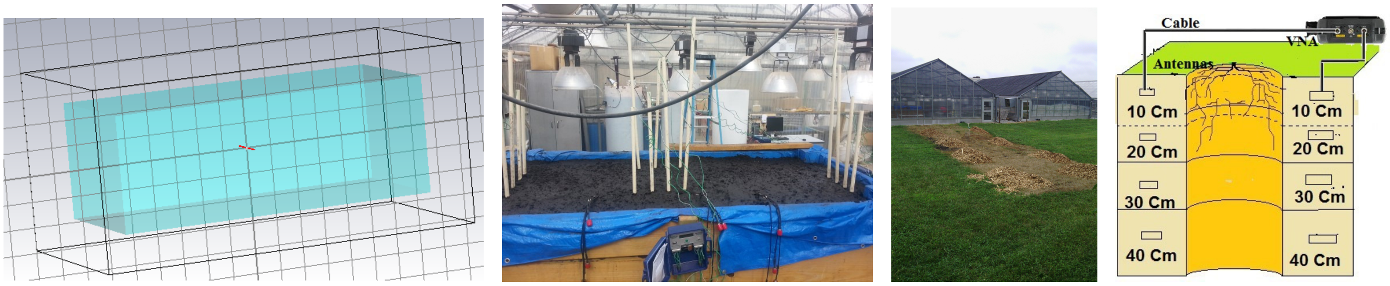

(a) (b) (c) (d)

Fig. 3: (a) CST MWS design of antenna buried in soil, (b) Indoor testbed, (c) Outdoor testbed in a field setting, (d) Experiment layout [48].

measurement data is shown to match well with sinusoidal current distribution. When the dipole antenna is buried underground, the current has the simple sinusoidal form with complex wave number of the soil k_s:

$$I_0(\zeta) = I_m \sin[k_s(l - |\zeta|)] \ , \tag{4}$$

where I_m is the amplitude of the current, l is the half length of the antenna, and $k_s = \beta_s + i\alpha_s = \omega\sqrt{\mu_0 \hat{\epsilon}_s}$ is the wave number in soil. $\mathbf{E_z}$ is given as:

$$\mathbf{E_z} = -\int_{-1}^{1} \frac{\mathbf{1}}{\mathbf{4\pi j\omega\epsilon_s}} \frac{\mathbf{e^{-jk_s r}}}{\mathbf{R}} \left(\frac{\partial^2}{\partial\zeta^2} + \mathbf{k_s^2}\right) \mathbf{I}(\zeta)\mathbf{d}\zeta, \tag{5}$$

By substituting the $\mathbf{E_z}$ in (5) and $\mathbf{I(0)}$ from (4) in (2) we get [34, Ch. 4]:

$$Z_a \approx f_1(\beta_s l) - i\left(120\left(\ln\frac{2l}{d} - 1\right)\cot(\beta_s l) - f_2(\beta_s l)\right) \ , \tag{6}$$

where

$$f_1(\beta_s l) = -0.4787 + 7.3246\beta_s l + 0.3963(\beta_s l)^2 + 15.6131(\beta_s l)^3 \tag{7}$$

$$f_2(\beta_s l) = -0.4456 + 17.0082\beta_s l - 8.6793(\beta_s l)^2 + 9.6031(\beta_s l)^3 \tag{8}$$

β_s is the real part of the wave number k_s, d is the diameter of the dipole, and l is half of the length of the dipole. βl is expressed as

$$\beta_s l = \frac{2\pi l}{\lambda_0} \mathrm{Re}\left\{\sqrt{\epsilon_s}\right\} \ , \tag{9}$$

where ϵ_s is the relative permittivity of soil and λ_0 is the wavelength in air. Since the permittivity of soil, ϵ_s, is frequency dependent, $\beta_s l$ is not a linear function of l/λ_0. Thus, when the antenna is moved from air to soil, not only its resonant frequency changes, but its impedance value at the resonant frequency also varies with the soil properties.

In a real deployment for IOUTs, sensor motes are buried at subsurface depths ($0.3\,\mathrm{m}$–$1\,\mathrm{m}$) [20]. At these depths, the environment cannot be modeled as homogeneous soil due to the impacts of soil-air interface. Next, we model the environment as a half-space consisting of air and soil to capture the impacts of the reflected waves from the soil-air interface on the impedance and return loss of the antenna.

We formulate the expression for mutual impedance of the underground dipole antenna by considering the effects of soil-air interface and burial depth of antenna. When a buried antenna is excited, a current distribution of $I_0(\zeta)$ is generated along the antenna (Fig. 2(a)). The generated wave propagates towards the soil-air interface, where it is reflected and refracted. The reflected electric field that reaches the antenna is denoted as E_r, which induces a current, I_r, on the antenna. The induced current further impacts the generated wave and higher order reflection effects exist. Due to the high attenuation in soil, these higher order effects are negligible and we consider only the first order effects in the following.

The induced current on the dipole, I_r, as well as the resulting impedance, Z_r, can be modeled as the result of a field generated by an *imaginary dipole* placed in a homogeneous soil environment. The distance of the two dipoles, h, is chosen such that E_r is the same at the real dipole. Based on this current distribution (4), the reflected E_r field from the soil-air interface at the antenna is [21, Ch. 7]:

$$E_r = -i30I_m\left(\frac{e^{-ik_s r_1}}{r_1} + \frac{e^{-ik_s r_2}}{r_2} - 2\cos k_s l \frac{e^{-ik_s r}}{r}\right) \times \Gamma \ , \tag{10}$$

where

$$r = [(2h)^2 + \zeta^2]^{1/2} \ , \tag{11}$$

$$r_1 = [(2h)^2 + (\zeta - l)^2]^{1/2} \ , \tag{12}$$

$$r_2 = [(2h)^2 + (\zeta + l)^2]^{1/2} \ , \tag{13}$$

h is the burial depth of the antenna, and Γ is the reflection coefficient at the soil-air interface, which is given by:

$$\Gamma = \frac{2}{1 + k_0/k_s} - 1 = \frac{2}{1 + \sqrt{\frac{1}{\epsilon_s}}} - 1 \ , \tag{14}$$

and k_0 is the wave number in air.

The expression for induced current on the UG dipole is given in Appendix B. Once I_r is determined, the antenna impedance is calculated as: $Z_a^u = Z_a.\frac{I_0}{I_r^2}$ and accordingly, the return loss of the antenna (in dB) is given by:

$$RL_{dB} = 20\log_{10}\left|\frac{Z_s + Z_a^u}{Z_s - Z_a^u}\right| \ , \tag{15}$$

where Z_s is the source impedance. The reflection coefficient Γ is given as: $|\Gamma| = 10^{\frac{RL}{20}}$. Reflection coefficient is transformed to impedance by using: $Z_a^u = Z_s\frac{1+\Gamma}{1-\Gamma}$. Standing wave ratio (SWR) is expressed as: $SWR = \frac{1+|\Gamma|}{1-|\Gamma|}$

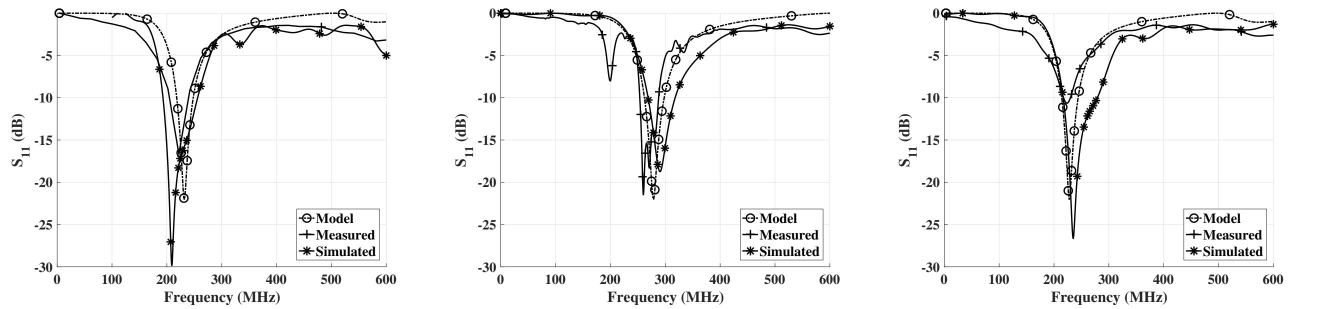

(a) Silt Loam (b) Sandy Soil (c) Silty Clay Loam

Fig. 4: Comparison of measured, simulated and theoretical return loss at 20 cm depth for 20% soil moisture in a) Silt Loam b) Sandy soil c) Silty clay loam soil.

B. Resonant Frequency of UG Dipole Antenna

The resonant frequency, f_r, is defined as the operation frequency where the input impedance of the antenna is the pure resistance, i.e.:

$$Z_a^u|_{f=f_r} = Z_r = R_a. \tag{16}$$

and where return loss is maximum such that [10]:

$$f_r = \max(RL_{dB}). \tag{17}$$

We also compare the performance of this analytical model by using the resonant frequency of an antenna designed based only on the soil permittivity by using: $f_r = f_0/\sqrt{\epsilon_s}$, where f_0 is the OTA resonant frequency, and ϵ_s is the permittivity of the soil.

C. UG Antenna Bandwidth

To find a closed-form formula for the bandwidth of the UG antenna is a challenging task since many factors such as soil moisture, soil type, permittivity, and burial depth are taken into account. However, based on the resonant frequency, we define the bandwidth expression. Over the resonant frequency, the bandwidth of the antenna is defined as the range of frequencies for which the antenna impedance is within a specified threshold. Accordingly, bandwidth (BW) is defined as [19]:

$$BW = \begin{cases} 0 & \text{if -}RL_{dB}(f) > \delta, \\ 2(f - f_m) & \text{if -}RL_{dB}(f) \leq \delta \text{ and } f < f_r, \\ 2(f_M - f) & \text{if -}RL_{dB}(f) \leq \delta \text{ and } f \geq f_r, \end{cases} \tag{18}$$

where f_r is the resonant frequency, f_m and f_M are the lowest and highest frequency at which $RL_{dB}(f) \leq \delta$. There is no fixed value of δ, and it depends on particular application. In literature, a value of $10\,\mathrm{dB}$ is generally used [10].

D. Model Evaluation Example

For the convenience of the reader, we present an example of the resonant frequency model evaluation in Table I.

TABLE I: An example of the model evaluation.

Input Parameter	Unit	Value
Clay particles	%	0.10
Sand particles	%	0.80
Bulk density	grams/cm^3	1.1
Solid soil particles	grams/cm^3	2.66
Depth	cm	20
Volumetric moisture content	%	20
Omega	rad/s	2π f
Velocity of light	m/s	3e8
Frequency	MHz	100-600
Antenna length	cm	8
Source impedance	ohm	50
Model Output		
Return Loss	dB	[0.0399....0.7703]
Resonant Frequency	MHz	211
Bandwidth	MHz	25

IV. Underground Dipole Antenna Simulations and Experiment Setup

To simulate an underground dipole antenna, CST Microwave Studio Suite (MWS) [13] is used. For controlled experiments, an indoor testbed has been designed [48]. Same antenna and soil parameters are simulated which are used in the testbed measurements. In Fig. 3(a), underground antenna simulation workspace has been shown. It can be observed that the simulation contains antenna inside the soil. Particle size distribution and classification of simulated soils is shown in Table II. Return loss measurement are conducted in an indoor testbed [49] and field settings under different volumetric water content (VWC). The indoor testbed is shown in Fig. 3(b).

To compare with the results of indoor testbed experiments and conduct underground-to-aboveground communications experiments, a testbed of dipole antennas has been prepared in an outdoor field with silty clay loam soil (Fig. 3(c)). Dipole antennas are buried in soil at a burial depth of $20\,\mathrm{cm}$ with distances from the first antenna as $50\,\mathrm{cm}$-$12\,\mathrm{m}$. Antenna S_{11} and frequency responses of the channel are measured using a Vector Network Analyzer (VNA). A diagram of the

TABLE II: Particle Size Distribution and Classification of Testbed Soils [48].

Textural Class	%Sand	%Silt	%Clay
Sandy Soil	86	11	3
Silt Loam	33	51	16
Silty Clay Loam	13	55	32

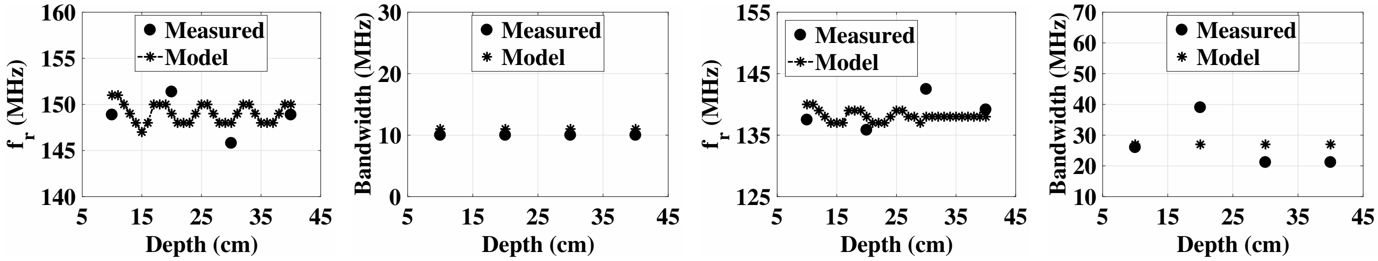

(a) Sandy (b) Sandy (c) Silt Loam (d) Silt Loam

Fig. 5: Comparison of measured and theoretical resonant frequency and bandwidth at different depths (40% VWC). a) Resonant frequency in sandy soil, b) Bandwidth in sandy soil, c) Resonant frequency in silt loam soil, c) Bandwidth in silt loam soil.

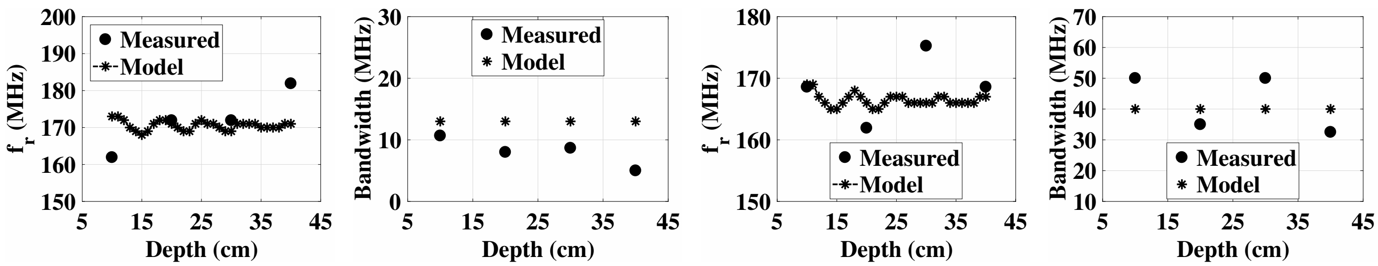

(a) Sandy (b) Sandy (c) Silt Loam (d) Silt Loam

Fig. 6: Comparison of measured and theoretical resonant frequency and bandwidth at different depths (30% VWC). a) Resonant frequency in sandy soil, b) Bandwidth in sandy soil, c) Resonant frequency in silt loam soil, c) Bandwidth in silt loam soil.

measurement layout is shown in Fig. 3(d). The coaxial cable is used to connect the VNA to the buried underground antenna. The dipole antenna is matched to 50 ohm. The balun is not used. Further details about experiment setup and methodology used can be found in [48].

V. Model Validation

A. Comparison of Theoretical, Simulated, and Measurement Results

In this section, we present the comparison of theoretical model, simulations, and measurements of dipole antenna for silt loam, silty clay loam, and sandy soil. Resonant frequency, bandwidth, and return loss at the resonant frequency are compared. To validate the theoretical analysis, we have conducted experiments in silty clay loam, sandy, and silt loam soil, by using the setup described in Section IV.

In Fig. 4(a), theoretical model and simulated results are compared with the measured return loss of antenna buried in silty clay soil at $20\,\mathrm{cm}$ depth at 20% soil moisture level. Measured return loss results agrees well with the model. Measured resonant frequency is 221 MHz and model value is 228 MHz. On the other hand, simulation results shows the resonant frequency at 210 MHz which is 11 MHz less than the measured return loss. Moreover, simulated return loss is also 7% lower at the resonant frequency as compared to measured and model return loss values at the resonance. This is caused by simulation uncertainties due to soil simulation in the simulator.

Return loss measurements at 20 cm depth in sandy soil are compared with theoretical and simulated results in Fig. 4(b). Measured, theoretical, and simulated resonant frequencies are within 1% difference range with measured resonant frequency at 283 MHz, model at 280 MHz and simulated at 286 MHz, respectively. Moreover, in sandy soil, only $1\,\%$ variations in return loss values at resonant frequency are observed as compared to the silt loam soil ($7\,\%$).

In Fig. 4(c), theoretical model, measured results, and simulations of antenna return loss are compared for the antenna buried in silty clay loam soil at $20\,\mathrm{cm}$ depth. Resonant frequency for both simulations and measurements is at 227 MHz and theoretical model value of resonant frequency is at 231 MHz, which is in agreement of all three results in the silty clay loam soil. These 1%-7% differences are mainly because of simulation effects in the software, as simulation setup can not realize the actual soil testbed scenario with maximum accuracy. Moreover, uncertainty in application of boundary conditions to the soil configurations in the software also lead to variations between measured and simulated results of the underground antenna in soil.

In Figs. 5-8, measured and theoretical resonant frequency and bandwidth at different depths in sandy and silt loam soil is compared for 10%-40% VWC range. At 40% VWC, in sandy soil (Fig. 5(a)), the measured resonant frequency value show a very good agreement with the model, where the resonant frequency is only $1.39\,\%$, $1.61\,\%$, $1.48\,\%$, $0.73\,\%$, different from the measured value of $148.9\,\mathrm{MHz}$, $151.4\,\mathrm{MHz}$, $145.8\,\mathrm{MHz}$, $148.9\,\mathrm{MHz}$, at $10\,\mathrm{cm}$ to $40\,\mathrm{cm}$ depths, respectively. The measured bandwidth in sandy soil (Fig. 5(b)) is also in very good agreement with the model value with only $1\,\mathrm{MHz}$ difference at all depths.

Similarly, at 40% VWC, in silt loam soil (Fig. 5(c)), the measured resonant frequency is only $1.78\,\%$, $1.59\,\%$, $4.01\,\%$, $0.08\,\%$, different from the measured value of $137.5\,\mathrm{MHz}$, $135.8\,\mathrm{MHz}$, $142.5\,\mathrm{MHz}$, $139.2\,\mathrm{MHz}$, at $10\,\mathrm{cm}$ to $40\,\mathrm{cm}$ depths, respectively. The measured bandwidth in silt loam

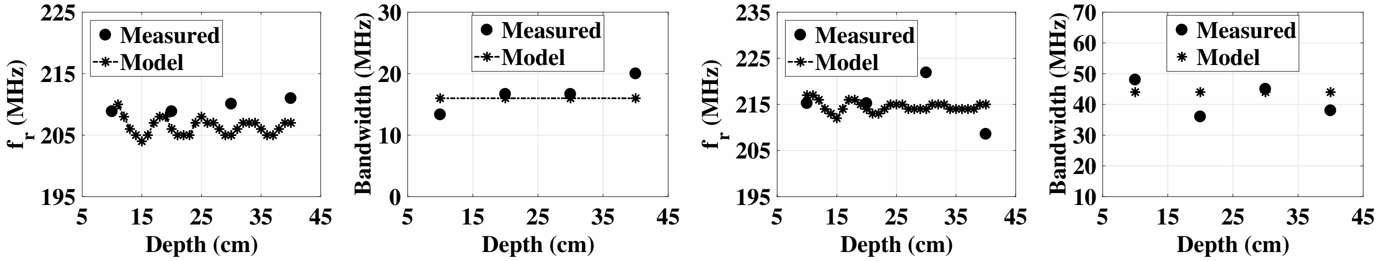

(a) Sandy (b) Sandy (c) Silt Loam (d) Silt Loam

Fig. 7: Comparison of measured and theoretical resonant frequency and bandwidth at different depths (20% VWC). a) Resonant frequency in sandy soil, b) Bandwidth in sandy soil, c) Resonant frequency in silt loam soil, c) Bandwidth in silt loam soil.

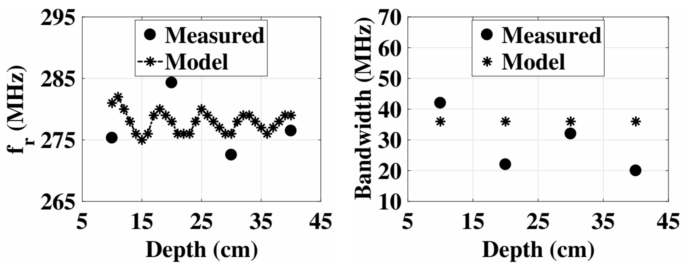

(a) Sandy (b) Sandy

Fig. 8: Comparison of measured and theoretical resonant frequency and bandwidth at different depths (10% VWC). a) Resonant frequency in sandy soil, b) Bandwidth in sandy soil.

(Fig. 5(d)) is 1 MHz, 7 MHz, 5.83 MHz, 5.83 MHz different from the model value at 10 cm-40 cm depths, respectively.

The comparison of measured and model resonant frequency and bandwidth at different depths in sandy soil at 30% VWC is given in Fig. 6(a)-6(b). The difference of measured and model resonant frequencies is 6.41 %, 0.58 %, 1.71 %, and 6.02 %, at 10 cm, 20 cm, 30 cm, and 40 cm depths, respectively. Similarly, the difference of measured and model bandwidth is 2.33 MHz, 5 MHz, 4.34 MHz, and 8 MHz, at 10 cm, 20 cm, 30 cm, and 40 cm depths, respectively.

In Fig. 6(c)-6(d), the comparison of measured and theoretical resonant frequency and bandwidth at different depths in silt loam soil at 30% VWC is given. The difference of measured and model resonant frequencies is 0.02 %, 2.46 %, 5.45 %, and 0.09 %, at 10 cm - 40 cm depths, respectively. The measured bandwidth in silt loam (Fig. 7(d)) is 10 MHz, 5 MHz, 10 MHz, and 7.5 MHz different from the model value at 10 cm-40 cm depths, respectively.

At 20% VWC, in sandy soil (Fig. 7(a)), the measured resonant frequency value show a very good agreement with the model, where the resonant frequency is only 0.01 %, 1.40 %, 2.48 %, and 1.93 %, different from the measured value of 208.9 MHz, 208.9 MHz, 210.1 MHz, and 211 MHz, at 10 cm to 40 cm depths, respectively. The measured bandwidth in sandy soil (Fig. 7(b)) is also in very good agreement with the model value with only 2.77 MHz, 0.67 MHz, 0.67 MHz, and 4 MHz difference at at 10 cm-40 cm depths, respectively.

Similarly, at 20% VWC, in silt loam soil (Fig. 7(c)), the measured resonant frequency is only 1.01 %, 0.47 %, 3.69 %, and 3.53 %, different from the measured value of 215.2 MHz, 215.2 MHz, 221.9 MHz, and 208.6 MHz, at 10 cm to 40 cm depths, respectively. Similarly, the difference of measured and modeled bandwidth is 4 MHz, 8 MHz, 1 MHz, and 6 MHz, at 10 cm - 40 cm depths, respectively.

In sandy soil at 10% VWC (Fig. 8(a)), the measured resonant frequency value show a very good agreement with the model, where the resonant frequency is only 2.24 %, 1.89 %, 1.66 %, and 1.25 %, different from the measured value of 275.3 MHz, 284.3 MHz, 272.6 MHz, and 276.5 MHz, at 10 cm to 40 cm depths, respectively. The measured bandwidth in sandy soil (Fig. 8(b)) is also in good agreement with the model value with only 6 MHz, 14 MHz, 2 MHz, and 16 MHz difference at at 10 cm-40 cm depths, respectively.

These variations in resonant frequency (up to 6.41 % in sandy soil and up to 5.45 % in silt loam) do not adversely impact the UG communications as bandwidth of the UG antenna (generally more than 20 MHz) [49] is higher than these variations in resonant frequency. Moreover, in this analysis, antenna bandwidth is calculated from the antenna return loss based on a threshold value (10 dB). Therefore, it is relative to the resonant frequency of the antenna. These differences in measured and model antenna bandwidth are caused by the variations in return loss shape and resonant frequency at a particular depth. Higher return loss and resonant frequency variations in soil lead to higher differences in antenna bandwidth.

It should be noted that since the theoretical resonant frequency model does not capture EM fields inside the coaxial cable connected to the antenna, the differences in resonant frequency between theory and experiment at different depths suggests that these variations are not caused by the soil medium but are primarily due to the coaxial cable effects. In theory, a perfect lossless transmission line is assumed, however, in practice, there are dielectric and conduction loss in a coaxial cable used in measurements. Due to fact that antennas are buried in the soil, it is not possible to take direct impedance measurements at antenna connectors and use of cables is inevitable. Therefore, the empirical resonant frequency clearly depends on the properties of the soil medium, depth, soil moisture but also on the coaxial cable used in these measurements. Moreover, difficulty in achieving the fine depth in soil due to moisture and compaction effects over time, also lead to deviations that occur at different depths. This is also consistent with the fact that effects of the soil-air interface impacts the resonant frequency of the underground antenna in soil and is ascribed to changes in the reflect field with depth. The soil-air interface effects are minimal when the transition

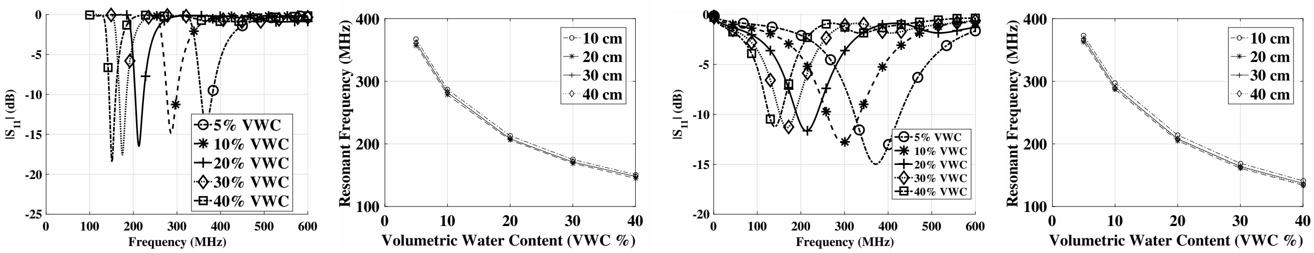

(a) Sandy (b) Sandy (c) Silt Loam (d) Silt Loam

Fig. 9: Theoretical return loss and resonant frequency in sandy, and silty clay loam soil at different burial depths. The depth for (a) and (c) is 20cm.

in resonant frequency is smooth from one depth to another depth and accordingly the effects of coupling are decreased as the depth changes (Fig. 6(a)). However, these effects can be more complicated to capture when phase change occurs in a smaller depth variation (Fig. 7(a)). Therefore, at these 10 cm, 20 cm, 30 cm, and 40 cm depths measured data provides a meaningful comparison with the theoretical results. In summary, change in the wave number, EM fields in coaxial cable and abrupt changes in phase and impedance with depth and soil interface effects are main factors of these differences in model and experimental data. Overall, the bandwidth and resonant frequency results show a very good agreement with the model. Additionally, the good fit with experimental results show that the model also captures the interface effects on the return loss of the antenna. Measured return loss values show the impacts of soil properties and soil moisture in the near vicinity of the antenna. Comparison of measurements with theoretical values makes the model a powerful analysis tool for the underground antenna.

B. Analysis of Impact of Operation Frequency

From an IOUT communication system design perspective, it is useful to analyze the performance of a dipole antenna return loss and resonant frequency in different soil types to get an insight for communication system design. In this section, first, the change in resonant frequency in different soils, under different soil moisture levels, for different operation frequencies, is analyzed through model evaluations. The connection of resonant frequency with the OTA frequency is also discussed. Then, we compare the model performance with the antenna designed based on the permittivity only, without consideration of the burial depth effects.

In Figs. 9(a)-9(b), where return loss, and resonant frequency is shown in sandy soil, it can be observed that with soil moisture increase from $5\,\%$ to $40\,\%$, resonant frequency decreases from $357\,\mathrm{MHz}$ to $146\,\mathrm{MHz}$ (59% decrease). Similarly, from Figs. 9(c)-9(d), return loss, and resonant frequency, in silt loam soil, is shown for soil moisture level of $5\,\%$-$40\,\%$. Resonant frequency decreases from $369\,\mathrm{MHz}$ to $137\,\mathrm{MHz}$ (62% decrease), when soil moisture increases from $5\,\%$ to $40\,\%$.

Ratio of resonant frequency of dipole antenna, $\frac{f_{rs}}{f_{ro}}$, in sandy, and silty clay loam soil to the OTA resonant frequency of the dipole antenna at $433\,\mathrm{MHz}$ and $915\,\mathrm{MHz}$ is shown in Fig. 10(a)-10(d), at different depths. f_{rs} and f_{ro} represents the resonant frequency in soil, and OTA, respectively. It can also be observed that with increase in soil moisture, $\frac{f_{rs}}{f_{ro}}$ becomes smaller (because resonant frequency decreases). Moreover, the It can be observed that $\frac{f_{rs}}{f_{ro}}$ ratio at $915\,\mathrm{MHz}$, as compared to the $433\,\mathrm{MHz}$, is not the same at different burial depths in both soils.

Soils are generally classified based on the percentage of clay, sand, and silt particles in soil using a soil textural triangle. Resonant frequency of soils in textural triangle are analyzed for volumetric water content range of 5% to 40% for a $433\,\mathrm{MHz}$ OTA antenna. Resonant frequency of different soils in textural triangle at different soil moisture levels are shown in Fig. 11. This antenna resonant frequency triangle can be used to predict the resonant frequency of an underground dipole antenna in different soils when soil type (sand, clay, silt particles) and soil water content is given.

Comparison of ratio of resonant frequency of a dipole antenna in soil to the OTA resonant frequency of the antenna in sandy, and silty clay loam soil is at $433\,\mathrm{MHz}$ and $915\,\mathrm{MHz}$ at different depths permittivity antenna is shown in Figs. 12(a)-12(d). Difference of change in resonant frequency is different at different depths, and this ratio also changes in comparison to the OTA. A more clear picture can be seen from the Figs. 13(a)-13(d), where difference in resonant frequency, Δ, of the resonant frequency of the theoretical model as compared to an antenna which is designed based on the soil permittivity only, is shown at different depths, at different soil moisture levels, in silty clay loam, and sandy soils, and at $433\,\mathrm{MHz}$ and $915\,\mathrm{MHz}$ frequencies. It can be observed that Δ is low at high soil moisture levels, and as soil moisture level decreases, Δ increases. Similarly, at $433\,\mathrm{MHz}$, Δ is low, and increases by $10\,\mathrm{MHz}$-$15\,\mathrm{MHz}$ at $915\,\mathrm{MHz}$ frequency. Hence, an IOUT system designed based on the permittivity $only$ will lead to performance degradation. Operation frequency is more probable to fall outside of the antenna bandwidth region, leading to minimal power transfer from antenna to the soil medium. It also underscores the effects of soil-air interface. Therefore, for an efficient power transfer, the antenna burial depth consideration is important in IOUT communications.

VI. Underground Wideband Antenna Design

In IOUT communications, two approaches can be used to mitigate the shift in resonant frequency of the underground dipole antenna. First approach is based on the software defined radio (SDR) operation, such that the operation frequency of the UG transceivers is adapted to soil moisture variations. Details of the cognitive wireless underground communications can be found in [19]. Second approach is based on the wideband operation, which we follow in this work. With insights gained from the analysis in shift of the underground dipole antenna, a

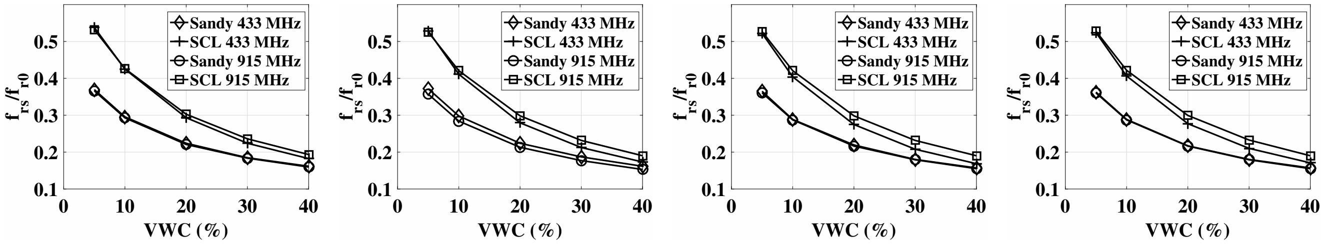

(a) 10 cm (b) 20 cm (c) 30 cm (d) 40 cm

Fig. 10: Ratio of resonant frequency in soil to the OTA resonant frequency of the antenna in sandy and silty loam soil is at 433 MHz and 915 MHz.

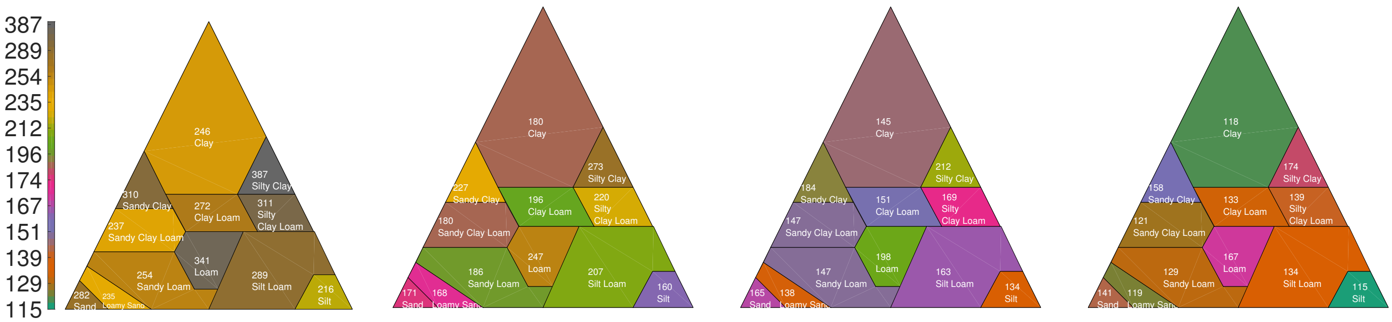

(a) 10% VWC (b) 20% VWC (c) 30% VWC (d) 40% VWC

Fig. 11: Resonant frequency (MHz) of different soils in textural triangle at different soil moisture levels for a 433 MHz OTA antenna

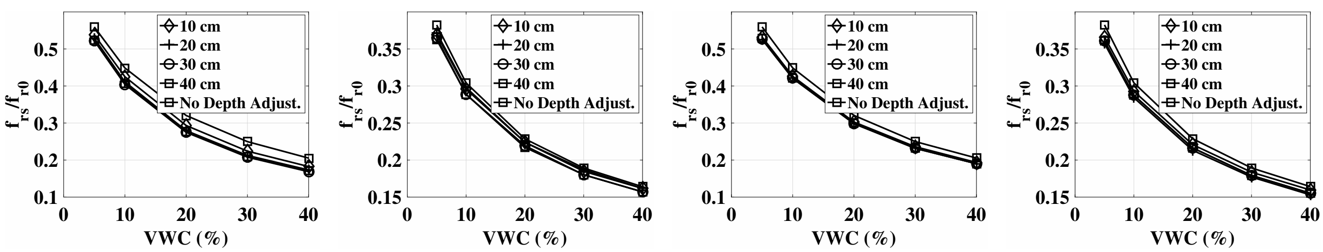

(a) SCL-433MHz (b) Sandy-433MHZ (c) SCL-915MHz (d) Sandy-915MHz

Fig. 12: Comparison of ratio of resonant frequency in soil to the OTA resonant frequency of the antenna in sandy and silty clay loam soil is at 433 MHz and 915 MHz at different depths with permittivity antenna.

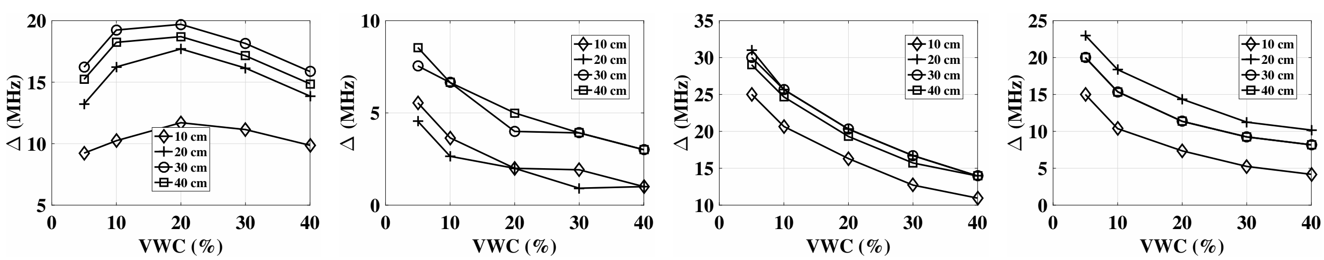

(a) SCL-433MHz (b) Sandy-433MHZ (c) SCL-915MHz (d) Sandy-915MHz

Fig. 13: Difference of the resonant frequency of the analytical model, Δ, as compared soil permittivity based antenna design.

wideband antenna has been designed [78]. This wideband antenna is capable of working across a wide range of frequencies. In this section, we design a wideband antenna for 433 MHz frequency, and results show that it has good performance in different soils. Different sizes of the wideband antenna based on the same design are designed and fabricated for testing. After experiments, the final design is chosen with a wideband plane of diameter 100 mm. The substrate of the antenna is a FR-4 material and its thickness is 1.6 mm. The feed line of the antenna is a coplanar waveguide structure. Further details about the antenna design can be found in [78]. The layout of the antenna is shown in Fig. 14(a).

A. Radiation Pattern for Underground Communications

In addition to the wide bandwidth of the wideband planar antenna, another advantage of using this antenna is its radiation pattern. For underground communications at this range of depth, there exist three paths [38]: direct wave, reflected wave and lateral wave as shown in Fig. 14(b). Of the three paths, lateral wave is dominant in the far field [20], [60], because the attenuation in air is much smaller than the attenuation in soil. Therefore, the radiation pattern of the antenna buried in soil should have a radiation pattern such that the lateral wave is maximized. It is shown in [38], [60], that lateral wave occurs only when the incident wave is at the critical angle θ_c, which is the angle above which no refraction exists.

The critical angle, θ_c, is a function of soil permittivity, which is a function of soil moisture. Hence, θ_c varies with the change in soil moisture. On the other hand, due to the fact that the relative permittivity of soil is ten to hundred times higher than air, θ_c is less than $15°$ in all soil moisture settings.

Based on this analysis, the desired radiation pattern of the underground antenna is unidirectional towards the soil-air interface. The beamwidth of the antenna should cover all the critical angles in different soil moisture values, which are in the range of $5°$ to $15°$. Thus, the planar antennas have desirable radiation patterns when they are placed parallel to the soil-air interface.

Moreover, the S-band contains the 2.4–2.483 GHz ISM band, widely used for low power unlicensed devices in precision agriculture such as data loggers, weather stations, farm machinery and equipment. Due to these facts, our design is compatible with these devices. We have presented a detailed survey in underground wireless technologies in [79].

B. The Return Loss

The performance of the antenna is tested in the same manner as in Section IV. Three antennas are buried at different depths: $0.13\,\mathrm{m}$, $0.3\,\mathrm{m}$, and $0.4\,\mathrm{m}$. During natural precipitation, return loss results for three soil moisture values, 10%, 30% and 40% are recorded. The return loss results of the designed antenna are shown in Fig. 15, where the return loss values at three different depths are depicted in Fig. 15(b) and the return loss values for the three soil moisture values are shown in Fig 15(c). The bandwidth analysis is also shown in Fig. 16. As shown in these figures, even though the resonant frequency varies in different situations, the return loss at $433\,\mathrm{MHz}$ is always below $10\,\mathrm{dB}$ for all the burial depth and soil moisture values.

C. Communication Results

The designed circular planar antenna is employed in our test bed to measure the communication quality of the underground-aboveground communications. For comparison, the $25\,\mathrm{mm}$ wideband antenna and the elliptical antenna are also employed. In these experiments, a mote with the planar antenna is buried at $40\,\mathrm{cm}$ depth and an aboveground mote with a directional Yagi antenna is employed to communicate with the underground mote for both the underground to aboveground channel (UG2AG) and aboveground to underground channel (AG2UG). The three antennas are attached to the same mote and buried at the same location for fair comparison. The received signal strength (RSS) values at different distance are recorded and depicted in Fig. 17. It can be observed that practical underground link distances are still limited to allow for practical multi-hop connectivity. Yet, communication ranges of up to 200 m is possible for aboveground communications.

It is shown that the $100\,\mathrm{mm}$ wideband antenna improves the communication range for both channels compared with the $25\,\mathrm{mm}$ circular and the elliptical antennas. For the UG2AG channel, the communication distance increases from $8\,\mathrm{m}$ (elliptical) and $17\,\mathrm{m}$ ($25\,\mathrm{mm}$ circular) to $55\,\mathrm{m}$. In other words, the designed antenna provides a 587.5% increase in communication range compared to the elliptical antenna and a 223.5% increase compared to the $25\,\mathrm{mm}$ circular antenna. For the AG2UG channel, the distance increases from $8\,\mathrm{m}$ (elliptical) and $15\,\mathrm{m}$ ($25\,\mathrm{mm}$ circular) to $55\,\mathrm{m}$, a 587.5% and a 266.7% increase, respectively. The results show that designing an antenna that is well matched in the soil environment is critical for the applications of IOUTs and can significantly increase the communication quality.

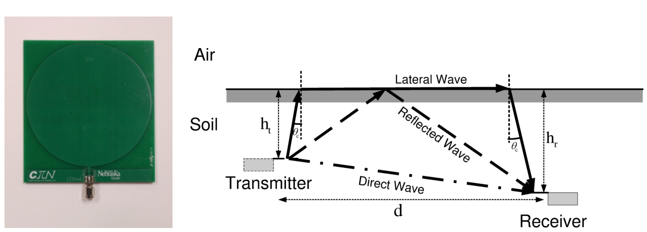

(a) (b)

Fig. 14: (a) UG wideband planar antenna, (b) The three paths of subsurface underground communication [20], [60].

D. Discussion

The proposed model can be utilized in two ways: 1) software defined radio, and 2) wide-band antenna design. For software defined radio, the approach is to adjust the operation frequency to the corresponding resonant frequency derived by the model output. Therefore, the matching circuit design is not required as the software defined radio works on software based signal processing. Second, regarding the wide-band antenna design, the bandwidth of this planar antenna is wide enough to accommodate the changes in the resonant frequency with change in soil moisture. In our wide-band antenna patent [78], we have shown that at some point, the permittivity (i.e., moisture content or other characteristic) may change. In response to detecting a threshold level of change in the permittivity of the dissipative medium, the antenna can maintain a particular level of return loss (e.g., less than -10 decibels) at the operation frequency. Maintaining or improving this level of return loss can ensure that wireless communications occur reliably and without interruption. The threshold level of change in the permittivity of the dissipative medium may be characterized by a five percent increase or decrease in the moisture level of the dissipative medium. In summary, we have highlighted these two approaches for underground communications and the particular and more specific design of the matching circuit is outside of the scope of the paper. The main motivation of the paper is the development of a model to predict the change in resonant frequency of an underground dipole antenna.

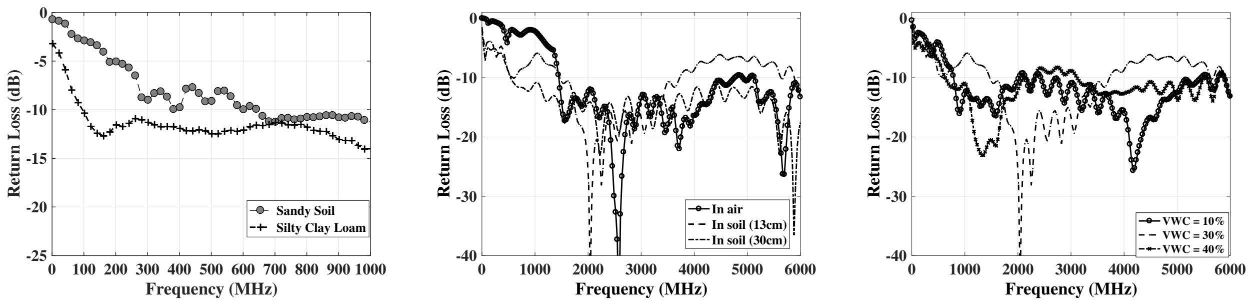

(a) (b) (c)

Fig. 15: The return loss results of the 100 mm wideband planar antenna: (a) in silty clay loam and sandy soil, (b) at different depths, (c) under different volumetric water content.

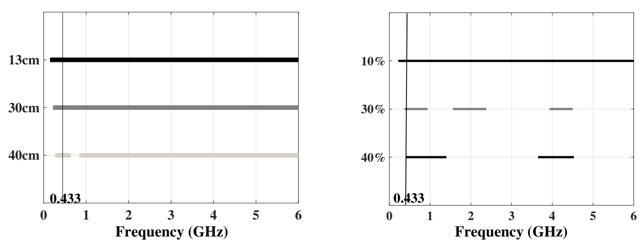

(a) (b)

Fig. 16: The bandwidth analysis of the 100 mm planar antenna at (a) three depths for soil moisture values of 10%, 30% and 40%, and (b) two soil moisture levels. The dashed line shows the bandwidth of the antenna.

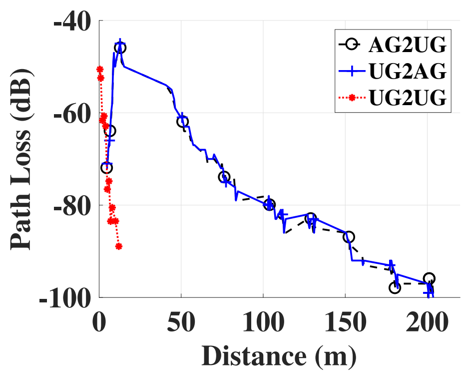

Fig. 17: The received signal strength at different distances for the underground to aboveground communication and aboveground to underground communication.

VII. Conclusions

In this paper, we investigated the effects of soil on antennas in underground communications. A model is developed to predict the resonant frequency of the UG antenna in different soils, at different depths, under water content variations. Theoretical analysis, simulations, and experimental validations are done to show that the high permittivity of the soil, and the effects of soil moisture variations mainly impact the performance of the antenna. The testbed and field experiments are conducted to further analyze these effects. The results show a very good agreement with the model. Moreover, the good fit with experimental results show that the model also captures the interface effects on the return loss of the antenna. Measured return loss values show the impacts of soil properties and soil moisture in the near vicinity of the antenna. Comparison of measurements with theoretical values makes the model a powerful analysis tool for the underground antenna design.

Appendix A
Dispersion in Soil

The effective permittivity of soil-water mixture, which is a complex number, can be modeled as [44]:

$$\epsilon_s = \epsilon_s' - i\epsilon_s'' \ , \tag{19}$$

$$\epsilon_s' = \begin{cases} 1.15\Big[1 + \rho_b/\rho_s\left(\epsilon_s^{\delta} - 1\right) + (m_v)^{\nu'}(\epsilon_{fw}')^{\delta} - \\ \quad m_v\Big]^{1/\delta} - 0.68 \qquad 0.3\,\text{GHz} \leq f \leq 1.4\,\text{GHz} \ , \\ \Big[1 + \rho_b/\rho_s\left(\epsilon_s^{\delta} - 1\right) + (m_v)^{\nu'}(\epsilon_{fw}')^{\delta} - m_v\Big]^{1/\delta} \\ \qquad\qquad 1.4\,\text{GHz} \leq f \leq 18\,\text{GHz} \ , \end{cases} \tag{20}$$

$$\epsilon_s'' = \Big[(m_v)^{\nu''}(\epsilon_{fw}'')^{\delta}\Big]^{1/\delta} \ , \tag{21}$$

where f is the frequency in Hz, ϵ_s is the relative complex dielectric constant of the soil-water mixture, m_v is the volumetric water content, ρ_b is the bulk density and ρ_s is the particle density, δ, ν' and ν'' are empirically determined soil-type dependent constants given by

$$\delta = 0.65 \ , \tag{22}$$

$$\nu' = 1.2748 - 0.519S - 0.152C \ , \tag{23}$$

$$\nu'' = 1.33797 - 0.603S - 0.166C \ , \tag{24}$$

where S and C represent the mass fractions of sand and clay, respectively. The quantities ϵ_{fw}' and ϵ_{fw}'' in (20) and (21) are the real and imaginary parts of the relative permittivity of free water, and are calculated from the Debye model [44]:

$$\epsilon_{fw}' = e_{w\infty} + \frac{\epsilon_{w0} - \epsilon_{w\infty}}{1 + (2\pi f \tau_w)^2} \ , \tag{25}$$

$$\epsilon_{fw}'' = \frac{2\pi f \tau_w(\epsilon_{w0} - \epsilon_{w\infty})}{1 + (2\pi f \tau_w)^2} + \frac{\delta_{eff}}{2\pi\epsilon_0 f}\frac{(\rho_s - \rho_b)}{\rho_s m_v} \ , \tag{26}$$

where $\epsilon_{w\infty} = 4.9$ is the limit of ϵ_{fw}' when $f \to \infty$, ϵ_{w0} is the static dielectric constant for water, τ_w is the relaxation time for water, and ϵ_0 is the permittivity of free space. Expressions for τ_w and ϵ_{w0} are given as a function of temperature. At room temperature (20°C), $2\pi\tau_w = 0.58 \times 10^{-10}$s and $\epsilon_{w0} = 80.1$.

The effective conductivity, δ_{eff}, in (26) in terms of the textural properties of the soil, is given by

$$\delta_{eff} = \begin{cases} 0.0467 + 0.2204\rho_b - 0.4111S + 0.6614C \\ \qquad\qquad 0.3\,\text{GHz} \leq f \leq 1.4\,\text{GHz} \; . \\ -1.645 + 1.939\rho_b - 2.25622S + 1.594C \\ \qquad\qquad 1.4\,\text{GHz} \leq f \leq 18\,\text{GHz} \; , \end{cases} \tag{27}$$

Wavenumber in soil is given as:

$$k_s = \beta_s + i\alpha_s \tag{28}$$

where β_s indicates phase shift and α_s indicates propagation losses. Alternatively

$$k_s = \omega\sqrt{\mu_0\epsilon_s} \tag{29}$$

where $\omega = 2\pi f$, and f is the frequency of the wave; μ_0 and ϵ_s are the permeability and permittivity of the soil, respectively. Next, current distribution along the UG dipole antenna is analyzed for calculating the antenna impedance.

Appendix B
Induced Current on UG Dipole

The induced current on the underground dipole, I_r, is modeled as:

$$I_r = \frac{E_r}{k_s} c(0) \frac{Z_0}{Z_0 + Z_s} \tag{30}$$

where k_s is the wave number in soil which depends on the soil moisture and soil type, and $c(0)$ is the induced current at the antenna for when Z_s is zero. $c(0)$ is approximated as [37]:

$$c(0) = \frac{i4\pi k_s}{\omega\mu_0}\left[\frac{1 - \cos k_s l}{\psi_{dUR}\cos k_s l - \psi_u(l)}\right] \tag{31}$$

where

$$\psi_{dUR} = \frac{\int_{-l}^{l}(\cos k_s z' - \cos k_s l)K(z,z')dz'}{\cos k_s z - \cos k_s l} \tag{32}$$

and

$$\psi_u = \int_{-l}^{l}(\cos k_s z' - \cos k_s l)K(l,z')dz' \tag{33}$$

where $K(z,z') = \frac{\exp(-1i.k_s.R)}{R}$ and $R = \sqrt{(l-z)^2 + a^2)}$.

Appendix C
Acknowledgments

The authors would like to thank the anonymous reviewers and the Editor for their valuable comments, especially for suggesting us to include an example which provided for a more self-contained paper.

This work is partially supported by a NSF CAREER award (CNS-0953900), NSF CNS-1423379, NSF CNS-1247941, CNS-1619285, and a NSF Cyber-Innovation for Sustainability Science and Engineering (CyberSEES) grant (DBI-1331895).

References

[1] T. E. Abrudan, O. Kypris, N. Trigoni and A. Markham, "Impact of Rocks and Minerals on Underground Magneto-Inductive Communication and Localization," in *IEEE Access*, vol. 4, no. , pp. 3999-4010, 2016.

[2] I. F. Akyildiz, P. Wang, and Z. Sun, "Realizing Underwater Communication through Magnetic Induction", *IEEE Communications Magazine*, Vol. 53, No. 11, pp. 42-48, November 2015.

[3] I. F. Akyildiz, Z. Sun, and M. C. Vuran, "Signal propagation techniques for wireless underground communication networks," *Physical Communication Journal (Elsevier)*, vol. 2, no. 3, pp. 167–183, Sept. 2009.

[4] I. F. Akyildiz and E. P. Stuntebeck, "Wireless underground sensor networks: Research challenges," *Ad Hoc Networks Journal (Elsevier)*, vol. 4, pp. 669–686, July 2006.

[5] A. Akdagli, "A closed-form expression for the resonant frequency of rectangular microstrip antennas" in *Microwave and Optical Technology Letters*, vol. 49, pp. 1848-1852, 2007.

[6] V. Arnautovski-Toseva and L. Grcev, "On the Image Model of a Buried Horizontal Wire," *IEEE Transactions on Electromagnetic Compatibility*, vol 58, no.1, pp.278-286, Feb. 2016.

[7] A. Banos, *Dipole radiation in the presence of a conducting halfspace*. Pergamon Press, 1966.

[8] K. Boyle, Y. Yuan, and L. Ligthart, "Analysis of mobile phone antenna impedance variations with user proximity," *Antennas and Propagation, IEEE Transactions on*, vol. 55, no. 2, pp. 364–372, Feb. 2007.

[9] A. W. Biggs, "Radiation fields from a horizontal electric dipole in a conducting half space," *IRE*, pp. 358, May. 1962.

[10] T. S. Bird, "Definition and Misuse of Return Loss [Report of the Transactions Editor-in-Chief]," *in IEEE Antennas and Propagation Magazine*, vol. 51, no. 2, pp. 166-167, April 2009.

[11] L. M. Brekhovskikh, *Waves in Layered Media*, Academic Press, New York, 1980.

[12] G. Castorina, L. Di Donato, A. F. Morabito, T. Isernia and G. Sorbello, "Analysis and Design of a Concrete Embedded Antenna for Wireless Monitoring Applications," in *IEEE Antennas and Propagation Magazine*, vol. 58, no. 6, pp. 76-93, Dec. 2016.

[13] CST Microwave Studio, Computer Simulation Technology. [Online]

[14] L. H. Dang, D. R. Jackson and J. T. Williams, "High power waveguide-fed reduced lateral wave antenna," *2010 IEEE Antennas and Propagation Society International Symposium*, Toronto, ON, July 2010

[15] T. Dissanayake, K. Esselle, and M. Yuce, "Dielectric loaded impedance matching for wideband implanted antennas," *IEEE Transactions on Microwave Theory and Techniques*, vol. 57, no. 10, pp. 2480–2487, Oct. 2009.

[16] M. Dobson, F. Ulaby, M. Hallikainen, and M. El-Rayes, "Microwave dielectric behavior of wet soil—part ii: Dielectric mixing models," *IEEE Transactions on Geoscience and Remote Sensing*, vol. GE-23, no. 1, pp. 35–46, January 1985.

[17] S. Dong, A. Yao, and F. Meng, "Analysis of an Underground Horizontal Electrically Small Wire Antenna," *Journal of Electrical and Computer Engineering*, vol. 2015, Article ID 782851, 9 pages, 2015.

[18] X. Dong and M. C. Vuran, and S. Irmak, " Autonomous precision agriculture through integration of wireless underground sensor networks with center pivot irrigation systems", in *Ad Hoc Networks*, vol. 11, no 7, pp. 1975-1987, Sep. 2013.

[19] X. Dong and M. C. Vuran, "Impacts of soil moisture on cognitive radio underground networks," in *IEEE BlackSeaCom 2013*, Batumi, 2013.

[20] X. Dong and M. C. Vuran, "A channel model for wireless underground sensor networks using lateral waves," in *IEEE Globecom '11*, Houston, TA, December 2011.

[21] R. S. Elliott, *Antenna Theory and Design*. Prentice-Hall, Inc., 1981.

[22] R. G. Fitzgerrell and L. L. Haidle , "Design and performance of four buried UHF antennas" , *IEEE Trans. Antennas Propagation* , vol. AP-20, no. 1, pp.56 -62 , 1972

[23] J. Galejs, *Antennas in Inhomogeneous Media*. Pergamon Press, 1969.

[24] J. Galejs, "Driving point impedance of linear antennas in the presence of a stratified dielectric," in *IEEE Transactions on Antennas and Propagation*, vol. 13, no. 5, pp. 725-737, Sep 1965.

[25] K. Gosalia, M. Humayun, and G. Lazzi, "Impedance matching and implementation of planar space-filling dipoles as intraocular implanted antennas in a retinal prosthesis," *IEEE Transactions on Antennas and Propagation*, vol. 53, no. 8, pp. 2365–2373, Aug. 2005.

[26] H. Guo, Z. Sun, J. Sun, and N. M. Litchinitser, "M2I: Channel Modeling for Metamaterial-Enhanced Magnetic Induction Communications", *IEEE Transactions on Antennas and Propagation*, Vol. 63, No. 11, pp. 5072-5087, November 2015.

[27] H. Guo and Z. Sun, "Channel and Energy Modeling for Self-Contained Wireless Sensor Networks in Oil Reservoirs", *IEEE Transactions on Wireless Communications*, Vol. 13, No. 4, pp. 2258-2269, April 2014.

[28] A. Guy, and G. Hasserjian, "Impedance properties of large subsurface antenna arrays," *IEEE Transactions on Antennas and Propagation*, vol. 11, no. 3, pp. 232–240, May. 1963.

[29] E. Hallen, "Theoretical investigation in the transmitting and receiving qualities of antennae," *Nova Acta Regiae Soc Sci Upsaliensis*, pp. 1-44, 11(4), 1938.

[30] R. Hansen, "Radiation and reception with buried and submerged antennas," in *IEEE Transactions on Antennas and Propagation*, vol. 11, no. 3, pp. 207-216, May 1963.

[31] K. Hunt, J. Niemeier, and A. Kruger, "RF communications in underwater wireless sensor networks," in *2010 IEEE International Conference on Electro/Information Technology (EIT)*, Normal, IL, May 2010.

[32] K. Iizuka, "An experimental investigation on the behavior of the dipole antenna near the interface between the conducting medium and free space," *IEEE Transactions on Antennas and Propagation*, vol. 12, no. 1, pp. 27–35, Jan. 1964.

[33] C. T. Johnk, *Engineering Electromagnetic Fields and Waves*, 2nd ed. John Wiley & Sons, Jan. 1988.

[34] R. C. Johnson, Ed., *Antenna Engineering Handbook*, 3rd ed. McGraw-Hill, Inc., 1993.

[35] A. S. Kesar, and E. Weiss, "Wave Propagation Between Buried Antennas," in *IEEE Transactions on Antennas and Propagation*, vol.61, no.12, pp.6152-6156, Dec. 2013.

[36] R. W. P. King, "The many faces of the insulated antenna," in *Proc. of the IEEE*, vol. 64, no. 2, pp. 228-238, Feb. 1976.

[37] R. W. P. King and G. S. Smith, *Antennas in Matter*. The MIT Press, Jan. 1981.

[38] R. W. P. King, M. Owens, and T. Wu, *Lateral Electromagnetic Waves*. Springer-Verlag, 1992.

[39] A. Konda, A. Rau, M. A. Stoller, J. M. Taylor, A. Salam, G. A. Pribil, C. Argyropoulos, and S. A. Morin, "Soft microreactors for the deposition of conductive metallic traces on planar, embossed, and curved surfaces," *Advanced Functional Materials*, vol. 28, no. 40, p. 1803020.

[40] S.-C. Lin, I. F. Akyildiz, P. Wang, and Z. Sun, "Distributed Cross-layer Protocol Design for Magnetic Induction Communication in Wireless Underground Sensor Networks", *IEEE Transactions on Wireless Communications*, Vol. 14, No. 7, July 2015.

[41] Mica family sensor motes. [Online]. Available: http://www.memsic.com

[42] R. K. Moore, and W. E. Blair, "Dipole radiation in conducting half space," *Journal of Res National Bureau of Standard*, 65D, pp. 547, 1961.

[43] K. A. Norton, "The Physical Reality of Space and Surface Waves in the Radiation Field of Radio Antennas," in *Proc. of the Institute of Radio Engineers*, vol. 25, no. 9, pp. 1192-1202, Sept. 1937

[44] N. Peplinski, F. Ulaby, and M. Dobson, "Dielectric properties of soil in the 0.3–1.3 ghz range," *IEEE Transactions on Geoscience and Remote Sensing*, vol. 33, no. 3, pp. 803–807, May 1995.

[45] J. Powell and A. Chandrakasan, "Differential and single ended elliptical antennas for 3.1-10.6 Ghz ultra wideband communication," in *Antennas and Propagation Society International Symposium*, vol. 2, Sendai, Japan, August 2004.

[46] C. J. Ritsema, H. Kuipers, L. Kleiboer, E. Elsen, K. Oostindie, J. G. Wesseling, J. Wolthuis, and P. Havinga, "A new wireless underground network system for continuous monitoring of soil water contents," *Water Resources Research Journal*, vol. 45, pp. 1–9, May 2009.

[47] N. Saeed, T. Y. Al-Naffouri, and M.-S. Alouini, "Towards the internet of underground things: A systematic survey," *arXiv preprint arXiv:1902.03844*, 2019.

[48] A. Salam, M. C. Vuran, and S. Irmak, "Pulses in the Sand: Impulse Response Analysis of Wireless Underground Channel," in *Proc. of 35th IEEE INFOCOM 2016*, San Francisco, CA, April 2016.

[49] A. Salam, and M. C. Vuran, "Impacts of Soil Type and Moisture on the Capacity of Multi-Carrier Modulation in Internet of Underground Things", in Proc. of the *25th ICCCN 2016*, Waikoloa, Hawaii, USA, Aug 2016. (Best Student Paper Award).

[50] A. Salam, M. C. Vuran, "Smart Underground Antenna Arrays: A Soil Moisture Adaptive Beamforming Approach", in Proc. of the *36th IEEE INFOCOM 2017*, Atlanta, GA, USA, May 2017.

[51] A. Salam, M. C. Vuran, "Wireless Underground Channel Diversity Reception With Multiple Antennas for Internet of Underground Things", in Proc. of the *IEEE ICC 2017*, Paris, France, May 2017.

[52] A. Salam, M. C. Vuran, and S. Irmak, "*Towards Internet of Underground Things in Smart Lighting: A Statistical Model of Wireless Underground Channel* ", in Proc. of the *14th IEEE International Conference on Networking, Sensing and Control (IEEE ICNSC)*, Calabria, Italy, May 2017.

[53] A. Salam, M. C. Vuran, "Smart Underground Antenna Arrays: A Soil Moisture Adaptive Beamforming Approach", Tech. Report, *Department of Computer Science and Engineering, university of Nebraska-Lincoln (TR-UNL-CSE-2017-0001)*, Jan 2017.

[54] A. Salam, M. C. Vuran, and S. Irmak, "Di-Sense: In situ real-time permittivity estimation and soil moisture sensing using wireless underground communications", *Computer Networks*, vol. 151, pp. 31-41, 2019.

[55] A. Salam, "Pulses in the sand: Long range and high data rate communication techniques for next generation wireless underground networks," *ETD collection for University of Nebraska - Lincoln*, no. AAI10826112, 2018. [Online]. Available: http://digitalcommons.unl.edu/dissertations/AAI10826112

[56] A. Salam, "Underground soil sensing using subsurface radio wave propagation," in *5th Global Workshop on Proximal Soil Sensing*, Columbia, MO, May 2019.

[57] A. Salam and S. Shah, "Urban underground infrastructure monitoring IoT: the path loss analysis," in *2019 IEEE 5th World Forum on Internet of Things (WF-IoT) (WF-IoT 2019)*, Limerick, Ireland, Apr. 2019.

[58] A. Salam and M. C. Vuran, "EM-Based Wireless Underground Sensor Networks," in *Underground Sensing*, S. Pamukcu and L. Cheng, Eds. Academic Press, 2018, pp. 247 – 285.

[59] A. Salam and S. Shah, "Internet of things in smart agriculture: Enabling technologies," in *2019 IEEE 5th World Forum on Internet of Things (WF-IoT) (WF-IoT 2019)*, Limerick, Ireland, Apr. 2019.

[60] D. Staiman and T. Tamir, "Nature and optimisation of the ground (lateral) wave excited by submerged antennas," in *Proc. of the Institution of Electrical Engineers*, vol. 113, no. 8, pp. 1299-1310, August 1966.

[61] A. Sommerfeld, "Uber die ausbreitung der Wellen in der drahtlosen Telegraphie". in *Ann. Phys* 28, pp. 665-737 (1909).

[62] N. Schemm, "A single-chip ultra-wideband based wireless sensor network node," Ph.D. dissertation, University of Nebraska-Lincoln, Dec. 2010.

[63] A. R. Silva and M. C. Vuran, "Communication with aboveground devices in wireless underground sensor networks: An empirical study," in *Proc. of IEEE ICC'10*, Cape Town, South Africa, May 2010, pp. 1–6.

[64] A. R. Silva and M. C. Vuran, "Development of a Testbed for Wireless Underground Sensor Networks," *EURASIP Journal on Wireless Communications and Networking*, vol. 2010, 2010.

[65] A. R. Silva and M. C. Vuran, "$(CPS)^2$: integration of center pivot systems with wireless underground sensor networks for autonomous precision agriculture," in *Proc. of ACM/IEEE International Conf. on Cyber-Physical Systems*, Stockholm, Sweden, April 2010, pp. 79–88.

[66] K. Sivaprasad, "An asymptomatic solution dipoles in a conducting medium," *IEEE Transactions on Antennas and Propagation*, vol. 11, no. 3, pp. 133, 1963.

[67] Z. Sun, I. F. Akyildiz, S. Kisseleff, and W. Gerstacker, "Increasing the Capacity of Magnetic Induction Communications in RF-Challenged Environments," *IEEE Transactions on Communications*, Vol. 61, No. 9, pp. 3943-3952, September 2013.

[68] Z. Sun, P. Wang, M. C. Vuran, M. A. Al-Rodhaan, A. M. Al-Dhelaan, I. F. Akyildiz, "MISE-PIPE: Magnetic induction-based wireless sensor networks for underground pipeline monitoring", *Ad Hoc Networks*, Volume 9, Issue 3, Pages 218-227, ISSN 1570-8705, 2011.

[69] Z. Sun, P. Wang, M. C. Vuran, M. A. Al-Rodhaan, A. M. Al-Dhelaan, I. F. Akyildiz, "BorderSense: Border patrol through advanced wireless sensor networks", *Ad Hoc Networks*, Volume 9, Issue 3, Pages 468-477, ISSN 1570-8705, 2011.

[70] C. T. Tai and R. E. Collin, "Radiation of a Hertzian dipole immersed in a dissipative medium," in *IEEE Transactions on Antennas and Propagation*, vol. 48, no. 10, pp. 1501-1506, 2000.

[71] X. Tan, Z. Sun, and I. F. Akyildiz, "Wireless underground sensor networks: MI-based communication systems for underground applications", *IEEE Antennas and Propagation Magazine*, Vol. 57, No. 4, pp. 74-87, August 2015.

[72] S. Temel, M. C. Vuran, M. M. Lunar, Z. Zhao, A. Salam, R. K. Faller, and C. Stolle, "Vehicle-to-barrier communication during real-world vehicle crash tests," *Computer Communications*, vol. 127, pp. 172 – 186, 2018. [Online]. Available: http://www.sciencedirect.com/science/article/pii/S0140366417305224

[73] M. J. Tiusanen, "Soil Scouts: Description and performance of single hop wireless underground sensor nodes", in *Ad Hoc Networks*, Volume 11, Issue 5, Pages 1610-1618, July 2013.

[74] M. J. Tiusanen, “Wideband antenna for underground Soil Scout transmission,” *IEEE Antennas and Wireless Propagation Letters*, vol. 5, no. 1, pp. 517–519, December 2006.
[75] M. J. Tiusanen, “Wireless Soil Scout prototype radio signal reception compared to the attenuation model,” *Precision Agriculture*, vol. 10, no. 5, pp. 372–381, November 2008.
[76] J. Toftgard, S. Hornsleth, and J. Andersen, “Effects on portable antennas of the presence of a person,” *IEEE Transactions on Antennas and Propagation*, vol. 41, no. 6, pp. 739–746, Jun. 1993.
[77] F. Tokan, N. T. Tokan, A. Neto and D. Cavallo, "The Lateral Wave Antenna," in *IEEE Transactions on Antennas and Propagation*, vol. 62, no. 6, pp. 2909-2916, June 2014.
[78] M. C. Vuran, X. Dong, and D. Anthony, "Antenna for wireless underground communication," *US Patent 9,532,118*, Dec 2016.
[79] M. C. Vuran, A. Salam, R Wong, and S Irmak, "Internet of Underground Things in Precision Agriculture: Architecture and Technology Aspects", Ad Hoc Networks (Elsevier), December 2018.
[80] M. C. Vuran, A. Salam, R. Wong, and S. Irmak, “Internet of underground things: Sensing and communications on the field for precision agriculture,” in *2018 IEEE 4th World Forum on Internet of Things (WF-IoT) (WF-IoT 2018)*, , Singapore, Feb. 2018.
[81] W. Wang, Z. Sun, and B. Zhu, "Modeling the Seismic Impacts on Communication Networks in Smart Grid", *International Journal of Distributed Sensor Networks*, vol. 2015, Article ID 587640, 2015.
[82] J. R. Wait, “The electromagnetic fields of a horizontal dipole in the presence of a conducting half-space,” *Canadian Journal of Physics*, vol. 39, no. 7, pp. 1017-1028, 1961.
[83] J. R. Wait, “Antennas in the geophysical environment-some examples,” in *Proc. of the IEEE*, vol. 80, no. 1, pp. 200-203, Jan 1992.
[84] H. A. Wheeler, “Useful radiation from an Underground Antenna” , *Journal of Research* , vol. 65D , no. 1, pp.89 -91 , 1961.
[85] T. T. Wu, and R. W. P. King, Lateral waves: new formulas for E1ϕ and E1z, *Radio Science*, 17(3), 532-538, 1982.
[86] H. Zemmour, G. Baudoin and A. Diet, "Soil Effects on the Underground-to-Aboveground Communication Link in Ultrawideband Wireless Underground Sensor Networks," in *IEEE Antennas and Wireless Propagation Letters*, vol. 16, no. , pp. 218-221, 2017.
[87] S. Zhong, G. Liu and G. Qasim, "Closed form expressions for resonant frequency of rectangular patch antennas with multidielectric layers," in *IEEE Transactions on Antennas and Propagation*, vol. 42, no. 9, pp. 1360-1363, Sep 1994.

Abdul Salam (S’04-M’18) (salama@purdue.edu) is an Assistant Professor in the Department of Computer and Information Technology at the Purdue University. His research involves underground soil sensing, wireless communications, Internet of Underground Things in digital agriculture, sensor-guided irrigation systems, and vehicular communications. He received his B.Sc. and MS degrees in Computer Sciences from Bahauddin Zakariya University, Multan, Pakistan in 2001 and 2004, respectively; and MS in Computer Engineering from UET, Taxila, Pakistan in 2012. He received his Ph.D. degree in Computer Engineering from the Cyber-Physical Networking Laboratory, Department of Computer Science and Engineering, University of Nebraska-Lincoln, Lincoln, NE, under the guidance of Professor Mehmet C. Vuran.

Abdul Salam has served in the Pakistan Army for 9 years in a number of command, staff, and field roles. He held the Principal position at the Army Public School and College, Thal Cantonment. Prior to his service at Pakistan Military, he was a lecturer at Department of Computer Science, Bahauddin Zakariya University, Multan; and Department of Computer Science and Information Technology, Islamia University, Bahawalpur, Pakistan. He is the recipient of ICCCN 2016 Best Student Paper Award, Robert B. Daugherty Water for Food Institute Fellowship, Gold Medal MS (CS) on securing first position in order of merit, and 2016-2017 Outstanding Graduate Student Research Award from Department of Computer Science and Engineering (CSE), University of Nebraska-Lincoln. Dr. Abdul Salam directs the Environmental Networking Technology (ENT) laboratory. He is the member of the Realizing the Digital Enterprise (RDE) research group and Center for Environment (C4E), a Purdue’s initiative for interdisciplinary, problem-driven research and teaching. He has served as an associate editor in IEEE GRSS Remote Sensing Code Library from 2016 to 2018. Currently, he serves as an Associate Editor of the Advanced Electromagnetics Journal.

Mehmet C. Vuran (S’98-M’07) (mcvuran@cse.unl.edu) received his B.Sc. degree in Electrical and Electronics Engineering from Bilkent University, Ankara, Turkey, in 2002. He received his M.S. and Ph.D. degrees in Electrical and Computer Engineering from the Georgia Institute of Technology, Atlanta, in 2004 and 2007, respectively, under the guidance of Prof. Ian F. Akyildiz. Currently, he is the Susan J. Rosowski Associate Professor of Computer Science and Engineering at the University of Nebraska-Lincoln and Robert B. Daugherty Water for Food Institute Fellow. He was awarded the Thomson Reuters Highly Cited Researcher award in 2014, 2015, and 206. He is the recipient of an NSF CAREER award in 2010 and the co-author of Wireless Sensor Networks textbook. His current research interests include wireless underground communications, agricultural Internet of Things, dynamic spectrum access in 5G networks, wearable embedded systems, connected autonomous systems, and cyber-physical networking. He is an Associate Editor of IEEE Transactions on Network Science and Engineering, Computer Networks Journal (Elsevier) and IEEE Communications Surveys and Tutorials.

Xin Dong is a member of technical staff at Riverbed Technology. He received his Ph.D. degree in computer engineering at the University of Nebraska-Lincoln in 2013 under the supervision of Dr. Vuran. He received the B.S. and M.E. degrees from Communication University of China in 2005 and 2007 respectively, both in communication engineering.

Christos Argyropoulos (S'04-M'11-SM'16) (christos.argyropoulos@unl.edu) received the Diploma of Electrical and Computer Engineering from the Aristotle University of Thessaloniki, Greece (2006). He holds a M.Sc. degree in Communication Engineering from the Microwaves and Communication Systems group of the University of Manchester, UK (2007) and a Ph.D. degree in Electronic Engineering from the Antennas and Electromagnetics Group of the Queen Mary, University of London, UK (2011). After completion of his PhD studies, he accepted a Postdoctoral Fellowship position in the University of Texas at Austin, USA. Next (2013), he worked as a Postdoctoral Associate in the Center for Metamaterials and Integrated Plasmonics at Pratt School of Engineering, Duke University, USA. From September 2014, he is an Assistant Professor at University of Nebraska-Lincoln, Department of Electrical Engineering, where he established the metamaterials and integrated nanophotonics lab.

He has published over 160 technical papers in highly ranked journals and refereed conference proceedings, including 5 book chapters. His main research interests include computational electromagnetics, numerical and analytical modeling of metamaterials and their applications, linear and nonlinear plasmonics, active metamaterials, novel antenna design, transformation optics, thermal emission from plasmonic structures, graphene nanophotonics, new energy harvesting devices and acoustic metamaterials. He has received several travel and research awards, such as 2017 URSI Young Scientist Award, 2017 ONR summer faculty fellowship, IEEE APS Junior Researcher Award of the 2013 Raj Mittra Travel Grant, EPSRC Research Scholarship, Royal Academy of Engineering international travel grant and twice the Marie Curie Actions Grant to attend the European School of Antennas. He has given several invited talks and seminars to different conferences and universities. He served as Student Paper Competition co-chair at IEEE APS 2016 and editor at the EPJ Applied Metamaterials special issue of the Metamaterials' Congress. He is a technical program committee member and special session on commercialization of metamaterials organizer at Metamaterials 2017 conference. He is Associate Editor at Optics Express and member of the Optical Society of America Traveling Lecturer program. He is treasurer at 16th Annual IEEE International Conference on Electro Information Technology. He is a senior member of IEEE, a full member of URSI Commission B, and member of IEEE Antennas and Propagation Society, IEEE Photonics Society, Optical Society of America, SPIE, American Physical Society and the Technical Chamber of Greece.

Suat Irmak has a doctorate in agricultural and biological engineering from the University of Florida. Suat Irmak's research, extension and educational programs apply engineering and scientific fundamentals in soil and water resources engineering, irrigation engineering and agricultural water management, crop water productivity, evapotranspiration and other surface energy fluxes for agro-ecosystems; invasive plant species water use; and impacts of changes in climate variables on water resources and agro-ecosystem productivity. Irmak leads the Nebraska Agricultural Water Management Network, which aims to increase adoption of new tools, technologies and strategies for increasing crop water productivity and reducing energy use in agriculture. He established the Nebraska Water and Energy Flux Measurement, Modeling and Research Network, made up of 12 water- and surface-energy flux towers forming a comprehensive network that measures surface energy and water vapor fluxes, microclimatic variables, plant physiological parameters and biophysical properties, water use efficiency, soil water content, surface characteristics and their interactions for various agro-ecosystems. He holds leadership roles in the American Society of Civil Engineers-Environmental and Water Resources Institute, for which he chairs the Evapotranspiration in Irrigation Hydrology Committee; American Society of Agricultural and Biological Engineers (ASABE); United States Committee on Irrigation and Drainage; and others. He has earned numerous awards and honors, including the ASABE New Holland Young Researcher Award and the ASABE Young Extension Worker Award.